The Determination of the Electromagnetic Field and *SAR* Pattern of an Interstitial Applicator in a Dissipative Dielectric Medium

YANG ZHANG, NILESH V. DUBAL, RANDALL TAKEMOTO-HAMBLETON, AND WILLIAM T. JOINES, MEMBER, IEEE

Abstract—**The spatial distribution of microwave energy absorbed per unit mass (the *specific absorption rate*, or *SAR*) in biological tissue is calculated for a class of interstitial antennas. The insulated interstitial applicator is simulated as an asymmetrically driven antenna. An expression for the electric field intensity near the antenna is derived and calculated by direct numerical evaluation of a surface integral over the insulation. The predicted *SAR* patterns obtained using the calculated electric field intensity and the tissue conductivity agree very well with the measured *SAR* distributions around three different applicators in muscle-equivalent phantoms.**

I. Introduction

INVASIVE applicators (or antennas) inserted directly into the tissue region to be heated often result in better control of the heating pattern, both inside and outside the target region, than would be obtained using noninvasive irradiation techniques. These interstitial, coaxial-line applicators are usually about 1 mm in diameter, have a radiating gap (or gaps) in the outer conductor, and are inserted into a plastic (good dielectric) catheter that is inserted into the region to be heated [1], [2]. The spatial distribution of energy absorbed per unit mass (the *specific absorption rate*, or *SAR* in W/kg) is directly related to the measurable temperature increase per unit time. However, adequate predictive models for calculating the *SAR* distribution for these applicators are needed and have not been developed previously.

In determining the *SAR* distribution, or heating pattern, of these antennas, the near field makes an important contribution. Recently, King *et al.* [3] calculated the electric field near an insulated symmetrical dipole in a dissipative medium. Their results, which were based upon an approximate numerical calculation, were improved by Casey [4] so that the near field of the dipole can be more precisely determined. In this paper, an asymmetrically driven antenna is used as a model of the interstitial applicator. This model was selected so that the two arms of the antenna would have different lengths, thus more closely simulating the physical arrangement of the interstitial applicator. The *SAR* distribution pattern along the antenna is determined by direct numerical evaluation of a surface integral over the insulation on the antenna. The calculated *SAR* patterns of three antennas agree very well with the measured patterns. Although the results presented in this paper are mainly directed toward applications in microwave hyperthermia, the field expressions are valid for obtaining both the near-field and far-field patterns of an asymmetrical dipole used for other purposes as long as the antenna is embedded in a dissipative medium. With the results presented in this paper, one is able to predict the heating or *SAR* pattern for interstitial applicators and the electromagnetic field distribution for insulated asymmetrical dipoles.

Manuscript received June 8, 1987; revised February 9, 1988, and May 13, 1988. This work was supported by the National Cancer Institute, DHHS, under PHS Grant 1 pol CA42745-01A1.

The authors are with the Department of Electrical Engineering, Duke University, Durham NC 27706.

IEEE Log Number 8823090.

II. The Properties of an Insulated Asymmetrical Dipole

An insulated asymmetrical dipole is shown in Fig. 1. It consists of two central conductors (region 1), of lengths h_1 and h_2 and radius a, surrounded by a cylinder of dielectric consisting of one or two layers (regions 2 and 3), respectively, of outer radii b and c. Outside this sheath of insulation is the infinite ambient medium (region 4). The central conductors are assumed to be perfect conductors. The wavenumbers of the insulating layers are given by $k_2 = \omega(\mu_0\epsilon_2)^{1/2}$ and $k_3 = \omega(\mu_0\epsilon_3)^{1/2}$, while the wavenumber in the ambient medium is $k_4 = \beta_4 + j\alpha_4 = \omega(\mu_0\tilde{\epsilon}_4)^{1/2}$, where $\tilde{\epsilon}_4 = \epsilon_4 + j\sigma_4/\omega$. A time dependence of $e^{j\omega t}$ is assumed for all fields.

The current distribution on an electrically thick, asymmetrically driven antenna has been approximately determined by King [5] and presented as a series of terms. For the special case of our electrically thin (length-to-diameter ratio greater than 15 [6]) asymmetrical dipole, we have found that a simpler current distribution will suffice for calculating the electromagnetic fields of interest. Based upon the current distribution along a section of suitably terminated, lossless, coaxial transmission line [7], the following current distribution on the asymmetrical dipole is

0018-9480/88/1000-1438$01.00

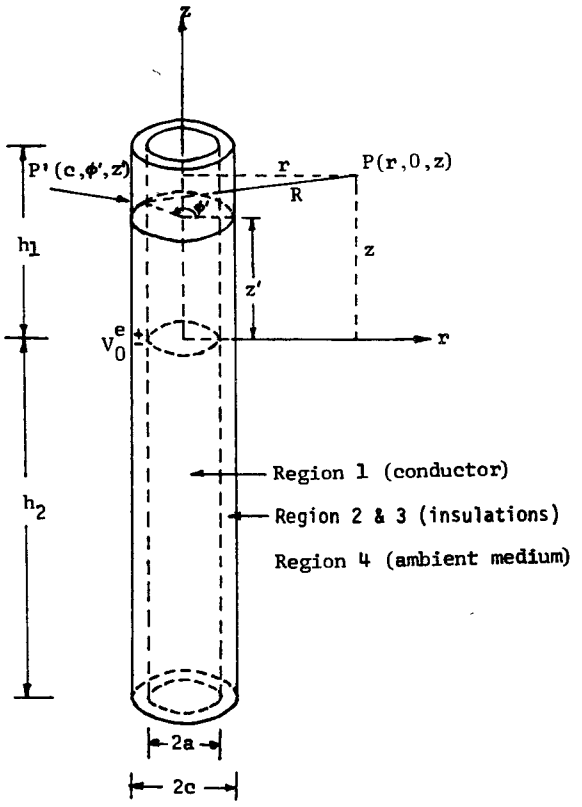

Fig. 1. Insulated asymmetrical dipole in ambient medium. The antenna is fed from the bottom through a coaxial cable.

assumed:

$$I_1(z) = I_0 \frac{\sin k_L(h_1 - z)}{\sin k_L h_1}, \qquad 0 \leqslant z \leqslant h_1 \tag{1}$$

$$I_2(z) = I_0 \frac{\sin k_L(h_2 + z)}{\sin k_L h_2}, \qquad -h_2 \leqslant z \leqslant 0 \tag{2}$$

where

$$I_0 = V_0^e / Z_A. \tag{3}$$

Here k_L is the complex wavenumber defined in [3]; Z_A is the impedance of the antenna; h_1 is the length of the tip, which is the extension of the inner conductor; and h_2 is the effective length of the outer conductor of the coaxial line. Due to the surrounding dissipative medium, we have assumed that the current distribution on the outside of the coaxial line vanishes at a distance h_2 from the gap. The value of h_2 is determined experimentally by two different methods that are described later. Equations (1) and (2) are valid subject to the following conditions:

$$|k_4/k_2|^2 \gg 1 \qquad |k_4/k_3|^2 \gg 1$$
$$(k_2 b)^2 \ll 1 \qquad (k_3 c)^2 \ll 1. \tag{4}$$

Note that (1) and (2) have already satisfied the following conditions required by the dipole [5]:

$$I_1(0) = I_2(0) \tag{5}$$

$$I_1(h_1) = 0 \qquad I_2(-h_2) = 0. \tag{6}$$

The impedance, Z_A, of the asymmetrical dipole can be approximately determined by the mean-value formula [8] as

$$Z_A = \frac{Z_1 + Z_2}{2} \tag{7}$$

where Z_1 and Z_2 denote the impedance of two center-driven symmetrical dipoles of half-length equal to h_1 and h_2, respectively. The formula for determining the impedance of a symmetrical dipole is given in [3].

The charge per unit length along the antenna is obtained from the continuity equation as

$$q_1(z) = \frac{-jdI_1(z)}{\omega\, dz} = \frac{jk_L I_0 \cos k_L(h_1 - z)}{\omega \sin k_L h_1}, \qquad 0 \leqslant z \leqslant h_1. \tag{8}$$

$$q_2(z) = \frac{-jdI_2(z)}{\omega\, dz} = \frac{-jk_L I_0 \cos k_L(h_2 + z)}{\omega \sin k_L h_2}, \qquad -h_2 \leqslant z \leqslant 0. \tag{9}$$

Since the field outside the insulator can be calculated accurately and simply by using an equivalent single layer, regions 2 and 3 are replaced with an effective single-layer insulator of permittivity ϵ_{2e} and wavenumber k_{2e} as defined in [3]. The cylindrical components of the electromagnetic field in the effective insulation ($a \leqslant r \leqslant c$) are approximated by the following expressions:

$$H_{21\phi}(r, z) \doteq \frac{I_1(z)}{2\pi r} = \frac{I_0 \sin k_L(h_1 - z)}{2\pi r \sin k_L h_1}, \qquad 0 \leqslant z \leqslant h_1 \tag{10}$$

$$H_{22\phi}(r, z) \doteq \frac{I_2(z)}{2\pi r} = \frac{I_0 \sin k_L(h_2 + z)}{2\pi r \sin k_L h_2}, \qquad -h_2 \leqslant z \leqslant 0 \tag{11}$$

$$E_{21r}(r, z) \doteq \frac{q_1(z)}{2\pi\epsilon_{2e} r} = \frac{jk_L I_0 \cos k_L(h_1 - z)}{2\pi\epsilon_{2e} r\omega \sin k_L h_1}, \qquad 0 \leqslant z \leqslant h_1 \tag{12}$$

$$E_{22r}(r, z) \doteq \frac{q_2(z)}{2\pi\epsilon_{2e} r} = \frac{-jk_L I_0 \cos k_L(h_2 + z)}{2\pi\epsilon_{2e} r\omega \sin k_L h_2}, \qquad -h_2 \leqslant z \leqslant 0 \tag{13}$$

$$E_{21z}(r, z) \doteq \int_a^r \left[\frac{\partial E_{21r}(r, z)}{\partial z} - j\omega\mu_0 H_{21\phi}(r, z)\right] dr = \frac{-j\omega\mu_0 I_0}{2\pi} \ln\left(\frac{r}{a}\right)\left(1 - \frac{k_L^2}{k_{2e}^2}\right) \frac{\sin k_L(h_1 - z)}{\sin k_L h_1}, \qquad 0 \leqslant z \leqslant h_1 \tag{14}$$

$$E_{22z}(r, z) \doteq \int_a^r \left[\frac{\partial E_{22r}(r, z)}{\partial z} - j\omega\mu_0 H_{22\phi}(r, z)\right] dr = \frac{-j\omega\mu_0 I_0}{2\pi} \ln\left(\frac{r}{a}\right)\left(1 - \frac{k_L^2}{k_{2e}^2}\right) \frac{\sin k_L(h_2 + z)}{\sin k_L h_2}, \qquad -h_2 \leqslant z \leqslant 0. \tag{15}$$

Equations (10)–(13) are quasi-static approximations while (14) and (15) are from one of Maxwell's equations by differentiation and integration [3].

III. The Electric Field in the Ambient Medium and Its Calculation

The electric field in the ambient medium is determined from the electromagnetic field at the surface of the insulation by the following integration [9]:

$$E_4(r,z)=\frac{1}{4\pi}\int_{-h_2}^{h_1}dz'\int_{-\pi}^{\pi}cd\phi'\Big[j\omega\mu_0 H_{4\phi}(c,z')\Psi a_{z'} - E_{4z}(c,z')a_{\phi'}\times\nabla'\Psi+E_{4r}(c,z')\nabla'\Psi\Big] \quad (16)$$

where

$$\Psi=\frac{e^{jk_4R}}{R} \quad (17)$$

and

$$R=\left[(z-z')^2+(r-r')^2+4rr'\sin^2\frac{\phi'}{2}\right]^{1/2}\Bigg|_{r'=c}. \quad (18)$$

Note that the contribution from both end surfaces of the insulation has been omitted in (16). The unprimed cylindrical coordinates refer to the observation point $P(r,\phi,z)$, while the primed coordinates (r',ϕ',z') are the source points. The operator ∇' is defined with respect to the primed coordinates as

$$\nabla'=\boldsymbol{a}_{r'}\frac{\partial}{\partial r'}+\boldsymbol{a}_{\phi'}\frac{1}{r'}\frac{\partial}{\partial\phi'}+\boldsymbol{a}_{z'}\frac{\partial}{\partial z'}.$$

The source fields in (16) are obtained from (10)–(15) with the following boundary conditions at $r=c$:

$$H_{4\phi}(c,z')=H_{2\phi}(c,z') \quad (19)$$

$$E_{4r}(c,z')=\frac{\epsilon_{2e}}{\tilde{\epsilon}_4}E_{2r}(c,z') \quad (20)$$

and

$$E_{4z}(c,z')=E_{2z}(c,z') \quad (21)$$

where

$$\frac{\epsilon_{2e}}{\tilde{\epsilon}_4}=\frac{\omega^2\mu_0\epsilon_{2e}}{\omega^2\mu_0\tilde{\epsilon}_4}=\frac{k_{2e}^2}{k_4^2}. \quad (22)$$

Owing to the rotational symmetry, all fields are independent of ϕ. Therefore, ϕ has been set equal to zero in (16).

Substituting (10)–(15) and (19)–(21) into (16), we find the components of the electric field as follows:

$$\begin{aligned}E_{4z}(r,z)&=\frac{I_0}{4\pi^2\sin k_Lh_1}\Bigg\{j\omega\mu_0\int_0^{h_1}\int_0^{\pi}\sin k_L(h_1-z')\frac{e^{jk_4R}}{R}d\phi'dz'\\&+j\omega\mu_0c\ln\left(\frac{c}{a}\right)\left(1-\frac{k_L^2}{k_{2e}^2}\right)\int_0^{h_1}\int_0^{\pi}\sin k_L(h_1-z')\\&\cdot\frac{e^{jk_4R}}{R^2}\left(\frac{1}{R}-jk_4\right)(c-r\cos\phi')\,d\phi'dz'\\&+\frac{jk_L}{\tilde{\epsilon}_4\omega}\int_0^{h_1}\int_0^{\pi}(z-z')\cos k_L(h_1-z')\\&\cdot\frac{e^{jk_4R}}{R^2}\left(\frac{1}{R}-jk_4\right)d\phi'dz'\Bigg\}\\&+\frac{I_0}{4\pi^2\sin k_Lh_2}\Bigg\{j\omega\mu_0\int_{-h_2}^{0}\int_0^{\pi}\sin k_L(h_2+z')\\&\cdot\frac{e^{jk_4R}}{R}d\phi'dz'\\&+j\omega\mu_0c\ln\left(\frac{c}{a}\right)\left(1-\frac{k_L^2}{k_{2e}^2}\right)\int_{-h_2}^{0}\int_0^{\pi}\sin k_L(h_2+z')\\&\cdot\frac{e^{jk_4R}}{R^2}\left(\frac{1}{R}-jk_4\right)(c-r\cos\phi')\,d\phi'dz'\\&-\frac{jk_L}{\tilde{\epsilon}_4\omega}\int_{-h_2}^{0}\int_0^{\pi}(z-z')\cos k_L(h_2+z')\\&\cdot\frac{e^{jk_4R}}{R^2}\left(\frac{1}{R}-jk_4\right)d\phi'dz'\Bigg\}\end{aligned} \quad (23)$$

and

$$\begin{aligned}E_{4r}(r,z)&=\frac{I_0}{4\pi^2\sin k_Lh_1}\Bigg\{j\omega\mu_0c\ln\left(\frac{c}{a}\right)\left(1-\frac{k_L^2}{k_{2e}^2}\right)\\&\cdot\int_0^{h_1}\int_0^{\pi}\sin k_L(h_1-z')\frac{e^{jk_4R}}{R^2}\left(\frac{1}{R}-jk_4\right)(z-z')\\&\cdot\cos\phi'\,d\phi'dz'\\&-\frac{jk_L}{\tilde{\epsilon}_4\omega}\int_0^{h_1}\int_0^{\pi}\cos k_L(h_1-z')\frac{e^{jk_4R}}{R^2}\left(\frac{1}{R}-jk_4\right)\\&\cdot(c\cos\phi'-r)\,d\phi'dz'\Bigg\}\\&+\frac{I_0}{4\pi^2\sin k_Lh_2}\Bigg\{j\omega\mu_0c\ln\left(\frac{c}{a}\right)\left(1-\frac{k_L^2}{k_{2e}^2}\right)\\&\cdot\int_{-h_2}^{0}\int_0^{\pi}\sin k_L(h_2+z')\frac{e^{jk_4R}}{R^2}\\&\cdot\left(\frac{1}{R}-jk_4\right)(z-z')\cos\phi'\,d\phi'dz'\\&+\frac{jk_L}{\tilde{\epsilon}_4\omega}\int_{-h_2}^{0}\int_0^{\pi}\cos k_L(h_2+z')\frac{e^{jk_4R}}{R^2}\left(\frac{1}{R}-jk_4\right)\\&\cdot(c\cos\phi'-r)\,d\phi'dz'\Bigg\}.\end{aligned} \quad (24)$$

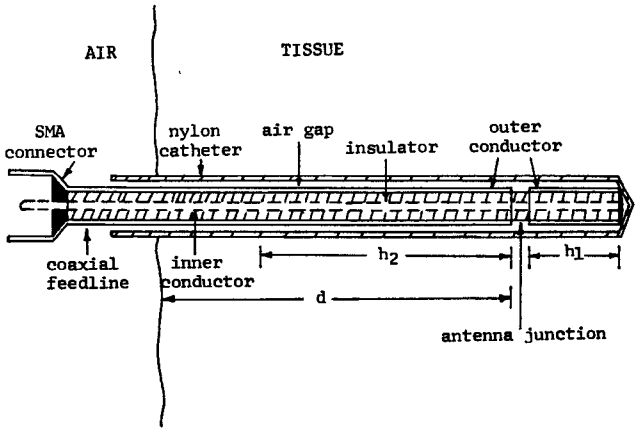

Fig. 2. An example of the interstitial applicator analyzed. h_1 and h_2 are, respectively, the lengths of the two active arms. The antenna fits into a blunt-ended nylon catheter.

The integrals in the above expressions for E_{4z} and E_{4r} must be evaluated numerically. In doing so, one has to evaluate double integrals of the form $\int_a^b\int_0^\pi f(\phi', z')\,d\phi'\,dz'$, where $f(\phi', z')$ is the real or imaginary part of a complex function with a pole at $\phi'=0$, $z'=z$, and $r=c$. An N-point Gaussian quadrature formula was used to evaluate the integration with respect to ϕ', i.e.,

$$\int_a^b\int_0^\pi f(\phi', z')\,d\phi'\,dz' = \frac{\pi}{2}\sum_{k=1}^{N} A_k \int_a^b f\left[\frac{\pi}{2}(x_k+1), z'\right] dz' \tag{25}$$

where x_k are the zeros of the Lengendre polynomial $P_N(x)$, and A_k are the corresponding weighting factors as tabulated in [10]. Because of the high peak nature of the integrand function, the resulting integrations with respect to z' in (25) were performed by using the adaptive Simpson's rule [11], [12]. This algorithm of integration has been proved to be very effective in integrating over a strongly peaked function.

The validity of the above derivations was checked by applying it to a symmetrical insulated dipole and comparing the calculated results with those in [4]. This was accomplished by setting $h_1=h_2=3.1$ cm with all other parameters the same as those in [4]. The values of power per unit volume of tissue as tabulated in [4, table I] were exactly reproduced. Therefore, the validity of the theoretical analysis and the computer program was confirmed. We then proceeded to analyze the asymmetrical dipole. The number of points in the Gaussian quadrature was determined by increasing the number until convergence was observed. It was found that a 40-point Gaussian quadrature was sufficient to produce acceptably accurate results.

IV. The Calculated *SAR* Distribution

Three applicators are used as examples in the determination of the field pattern. The antennas are thin enough to be inserted into a catheter embedded in tumor tissue, as shown in Fig. 2, where h_1 and h_2 are the lengths of the two active arms of the antenna, and d is the distance from the gap to the air–tissue interface. Two of the applicators were constructed from semirigid microwave coaxial cable (Microcoax, UT-34M), which has an outer radius $a=0.475$ mm. The tip lengths of the applicators, h_1, are 1.5 cm and 2.0 cm, respectively. The other applicator is commercially available (Clinitherm Co.); it has a tip length h_1 of 3.5 cm and an outer radius $a=0.470$ mm. The insulating dielectric has two layers. The inner layer of air between the antenna and the catheter has an outer radius $b=0.584$ mm and a relative permittivity $\epsilon_{2r}=1$. The outer layer of insulation is the catheter (INSYTE, 16GA, Deseret Med. Inc.) of outer radius $c=0.80$ mm and relative permittivity $\epsilon_{3r}=3.5$ [13]. The ambient medium is phantom muscle tissue of relative permittivity $\epsilon_{4r}=51.0$ and conductivity $\sigma_4=1.28$ S/m. The antenna is operated at 915 MHz with V_0^e assumed to be 1 V. Note that the conditions (4) are well satisfied by this system.

To evaluate the electric field components in (23) and (24), we must first determine the active length, h_2, of the applicators. In order to achieve this, the applicators with catheters were inserted into phantom muscle tissue. The return loss at the input to the applicators was monitored on a network analyzer (HP8754A) while increasing the depth d. It was found that when $d \geq 10$ cm, the return loss stays at 24 ± 2 dB for the applicator of $h_1=2.0$ cm, indicating that the active length h_2 is approximately $5h_1$ or 10 cm for this applicator. It was found, in the same way, that the active length h_2 is approximately $7h_1$ or 10.5 cm for the applicator of $h_1=1.5$ cm, and $4h_1$ or 14.0 cm for the one with $h_1=3.5$ cm. This is the first of two different experimental methods used to determine the active length h_2. It should be noted that the effective length, h_2, depends not only on the properties of the antenna but also on the attenuation of the medium.

The primary quantity of interest in hyperthermia applications is the rate of heat generation as a function of position relative to the antenna. The *SAR* in W/kg is given by

$$SAR = \frac{\sigma_4}{2\rho}E_4\cdot E_4^* = \frac{\sigma_4}{2\rho}\left(|E_{4r}|^2+|E_{4z}|^2\right) \tag{26}$$

where σ_4 is the electrical conductivity of the ambient medium and ρ is the density of the medium. For phantom muscle, $\rho=970$ kg/m^3. The calculated *SAR* distributions at $r=5$ mm versus the relative position of the three applicators are plotted as solid lines in Figs. 3, 4, and 5, where the *SAR* values are normalized to their maximum values, respectively, since the exact value of the potential, V_0^e, across the gap is not known. In these figures, the gaps in the outer conductors of applicators are at $z=0$. A second experimental method was used to find the value of h_2. In Figs. 3, 4, and 5, the value of h_2 used in the calculations was determined by varying h_2 through a range of values to give the best agreement between the calculated and measured *SAR* distributions. The two experimental methods yielded essentially the same values of h_2. In Fig. 3, $h_1=1.5$ cm, and the predicted *SAR* pattern with $h_2=7h_1$ peaks at about $z=-1.0$ cm. In Fig. 4, $h_1=2.0$ cm, and the predicted *SAR* pattern with $h_2=5h_1$ peaks at

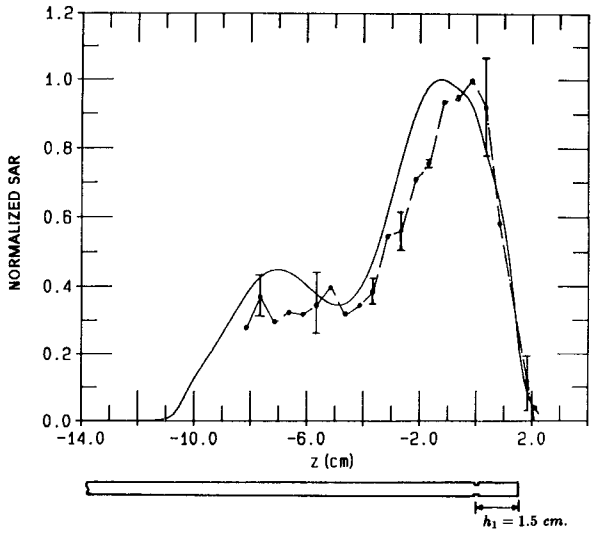

Fig. 3. Normalized *SAR* distribution at $r = 0.5$ cm versus the relative position along the antenna in phantom muscle. Solid line: calculated curve. Dotted line: measured curve. $h_1 = 1.5$ cm.

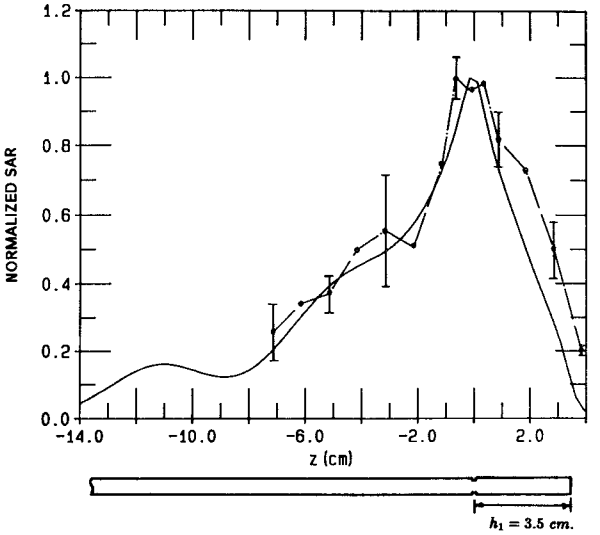

Fig. 5. Normalized *SAR* distribution at $r = 0.5$ cm versus the relative position along the antenna in phantom muscle. Solid line. calculated curve. Dotted line: measured curve. $h_1 = 3.5$ cm.

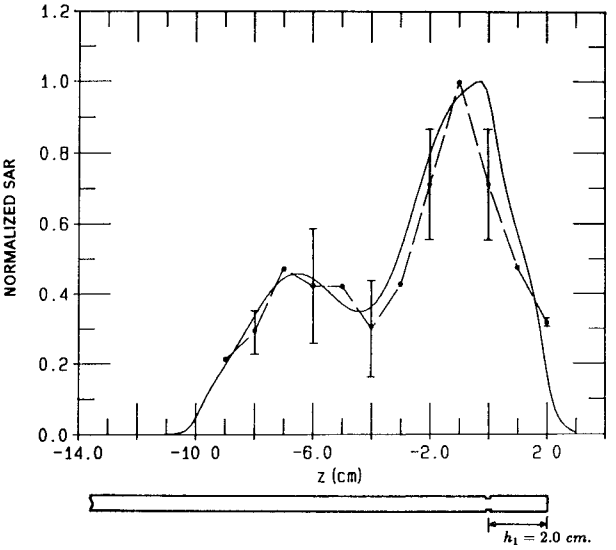

Fig. 4. Normalized *SAR* distribution at $r = 0.5$ cm versus the relative position along the antenna in phantom muscle. Solid line: calculated curve. Dotted line: measured curve. $h_1 = 2.0$ cm.

about $z = -0.5$ cm. Fig. 5 shows the *SAR* distribution of the Clinitherm applicator with $h_1 = 3.5$ cm, and $h_2 = 4h_1$ for the predicted *SAR*. Both the predicted and measured SAR patterns have a peak at $z = 0.0$ cm, but the patterns are spread over a greater length than for the two shorter applicators.

V. The *SAR* Measurements and Discussion

The experimental arrangement for measurement of *SAR* distribution is shown in Fig. 6. In this test setup, the microwave power at 915 MHz is applied from the microwave power generator through a dual-directional coupler (HP778D) with two power meters (HP435A) for monitoring forward and reflected power, to the applicator inserted into a catheter (INSYTE, 16GA, Deseret Med. Inc.) that is embedded in phantom muscle tissue. (Reference [14] gives the formulation of the phantom muscle tissue.) The temperature measurements were accomplished by a multichannel fluoroptic thermometer (Luxtron, model 3000) controlled by a computer (DEC MicroVAX II). A catheter is embedded in the tissue at 5 mm away, and in parallel with the applicator. This allows a temperature probe to move inside the catheter for monitoring the temperature at different points. The temperature probe inside the catheter is positioned by a computer-controlled stepper motor. The time rate of temperature increase for several fixed positions along the antenna was recorded by the system following a step application of microwave power. The step input power to the antenna was 10 W. Heating time was 20 seconds.

The specific absorption rate can be derived from the initial rise in temperature through the equation

$$SAR = kc\frac{\Delta T}{\Delta t} \tag{27}$$

where $k = 4186$ J/kcal, c is the specific heat of the tissue in kcal/kg°C ($c = 0.84$ kcal/kg°C for phantom muscle tissue), ΔT is the temperature rise in °C, and Δt is the measurement interval in seconds. Hence, *SAR* in (27) is in W/kg.

The measured *SAR* distributions of the three applicators, along the antenna lengths, are illustrated as a dotted line in Figs. 3, 4, and 5, respectively. The error bars are also shown in the figures. The measured *SAR* distributions have been normalized to their maximum value to make the comparison meaningful. Figs. 3, 4, and 5 show a very good agreement between the theoretical predictions and the measurements. A part of the difference between the theoretical and measured *SAR* distributions may be due to inaccurate positioning of the temperature probe relative to the position of the applicators. For instance, the measured *SAR* pattern in Fig. 3 is constantly shifted toward the right. But a similar phenomenon does not occur in Figs. 4

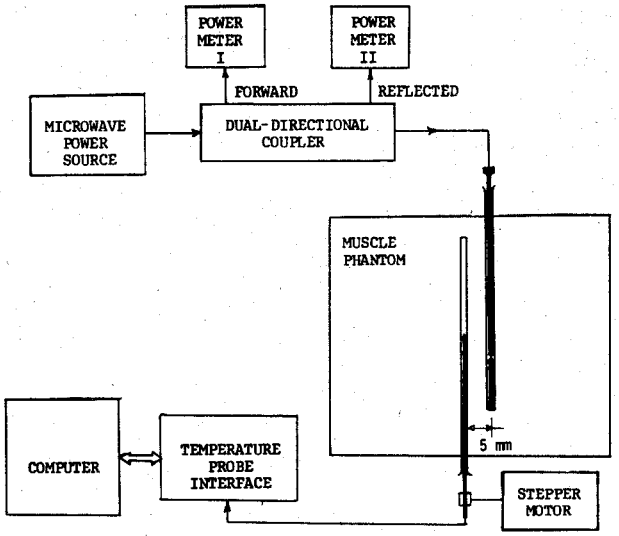

Fig. 6. The experimental arrangement for *SAR* measurements in phantom muscle.

and 5. This indicates that the temperature probe is off position along the catheter of the temperature probe. When account is taken of the differences, the agreement is quite satisfactory, and well within the experimental error. For the applicator with short tips (Figs. 3 and 4), a secondary peak was found at about $z = -7.0$ cm. But the heating zone is well localized. The applicator with a longer tip (Fig. 5) has no secondary peak, but the heating pattern spreads out over a wide region. Both the computed and the measured *SAR* patterns of the three applicators indicate that the maximum power deposition occurs near the gaps of the antennas.

VI. Conclusion

The electric field near an insulated asymmetrical dipole in a dissipative dielectric medium has been calculated by the direct numerical evaluation of a surface integral over the insulation. A comparison of the computed *SAR* results with the experimental measurements shows a very good agreement, lending support to the validity of the theoretical analysis. By the application of the methods presented in this paper, field patterns of any insulated, asymmetrical dipole or the *SAR* pattern of any interstitial applicator for hyperthermia may be predicted at any frequency, provided that the conditions in (4) are satisfied. The results presented in this paper will also allow us to predict the field pattern of an array of three or four insulated antennas. This study is planned for presentation in a subsequent paper.

References

[1] J. W. Strohbehn, E. D. Bowers, J. E. Walsh, and E. B. Douple, "An invasive microwave antenna for locally-induced hyperthermia for cancer therapy," *J. Microwave Power*, vol. 14, pp. 339–350, 1979.

[2] B. E. Lyons, R. H. Britt, and J. W. Strohbehn, "Localized hyperthermia in the treatment of malignant brain tumors using an interstitial microwave antenna array," *IEEE Trans. Biomed. Eng.*, vol. BME-31, pp. 53–62, Jan. 1984.

[3] R. W. P. King, B. S. Trembly, and J. W. Strohbehn, "The electromagnetic field of an insulated antenna in a conducting or dielectric medium," *IEEE Trans. Microwave Theory Tech.*, vol. MTT-31, pp. 574–583, July 1983.

[4] J. P. Casey and R. Bansal, "The near field of an insulated dipole in a dissipative dielectric medium," *IEEE Trans. Microwave Theory Tech.*, vol. MTT-34, pp. 459–463, Apr. 1986.

[5] R. W. P. King, "Asymmetrically driven antennas and the sleeve dipole," *Proc. IRE*, vol. 38, pp. 1154–1164, Oct. 1950.

[6] H. Jasik, *Antenna Engineering Handbook*. New York: McGraw-Hill, 1961, ch. 3, p. 3-2.

[7] R. W. P. King, R. B. Mack, and S. S. Sandler, *Arrays of Cylindrical Dipoles*. Cambridge: Cambridge University Press, 1968, ch. 2.

[8] H. Jasik, *Antenna Engineering Handbook*. New York: McGraw-Hill, 1961, ch. 3.

[9] S. Silver, *Microwave Antenna Theory and Design*. New York: Dover, 1965, ch. 3.

[10] M. Abramowitz and I. A. Stegun, *Handbook of Mathematical Functions*. Washington, DC: National Bureau of Standards, AMS 55, U.S. Dept. of Commerce, 1964, pp. 916–919.

[11] W. M. McKeeman, "Adaptive numerical integration by Simpson's rule," *Commun. Ass. Comput. Mach.*, vol. 5, Dec. 1962.

[12] W. M. McKeeman and L. Tester, "Nonrecursive adaptive Integration," *Commun. Ass. Comput. Mach.*, vol. 6, p. 315, June 1963.

[13] N. N. Rao, *Elements of Engineering Electromagnetics*, 2nd ed. Englewood Cliffs, NJ: Prentice-Hall, 1987, ch. 2, p. 90.

[14] C. K. Chou, G. W. Chen, A. W. Guy, and K. H. Luk, "Formulas for preparing phantom muscle tissue at various radiofrequencies," *Bioelectromagnetics*, vol. 5, no. 4, pp. 435–441, 1984.

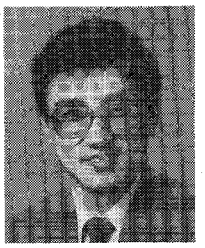

Yang Zhang was born in Shenyang, China, on December 5, 1957. He received the B.S.E.E degree (with high honors) from Chengdu Institute of Radio Engineering, Chengdu, China, in 1982, and the M.S. degree in electrical engineering from Duke University, Durham, NC, in 1984. He is presently with the Department of Electrical Engineering, Duke University, as a Research Assistant, where he is working towards the Ph.D. degree in microwave engineering. His research interests are in the area of electromagnetic wave interactions with materials, with applications to transmission lines, antennas, and microwave-induced hyperthermia.

Mr. Zhang is a member of Eta Kappa Nu.

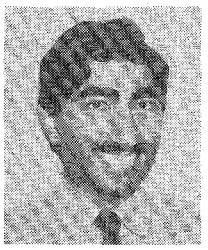

Nilesh V. Dubal received the B.S. and M.S. degrees in electrical engineering from Duke University, Durham, NC. His areas of interest include hyperthermia and the medical uses of microwave radiation. He is currently attending the Bowman Gray School of Medicine.

Randall Takemoto-Hambleton was born in Honolulu, Hawaii, on March 26, 1961. He received the B.S.E.E degree from the School of Engineering at Duke University in 1984. Currently he is a Research Assistant in the Department of Electrical Engineering at Duke University, where he is working towards the M.S.E.E. degree in microwave engineering. His research interests are in the area of electromagnetic wave interactions with materials, with emphasis on numerical modeling of electromagnetic field problems.

Mr. Takemoto-Hambleton is a member of Eta Kappa Nu.

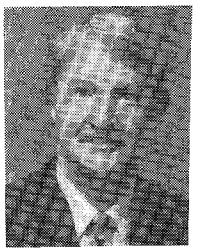

William T. Joines (M'61) was born in Granite Falls, NC, on November 20, 1931. He received the B.S.E.E. degree (with high honors) from North Carolina State University, Raleigh, in 1959, and the M.S. and Ph.D. degrees in electrical engineering from Duke University, Durham, NC, 1961 and 1964, respectively.

From 1959 to 1966, he was a member of the Technical Staff at Bell Laboratories, Winston-Salem, NC, where he was engaged in research and development of microwave components and systems for military applications. He joined the faculty of Duke University in 1966, and is currently a Professor of Electrical Engineering. His research and teaching interests are in the area of electromagnetic wave interactions with materials.